The Astrophysical Journal Letters, 890:L13 (7pp), 2020 February 10 https://doi.org/10.3847/2041-8213/ab71fd

A New Mechanism for Maunder-like Solar Minima: Phase Synchronization Dynamics in a Simple Nonlinear Oscillator of Magnetohydrodynamic Rossby Waves

Breno Raphaldini[1], Everton Medeiros[2], Carlos F. M. Raupp[1], and Andre Seiji Teruya[1]
[1] Instituto de Astronomia, Geofísica e Ciências Atmosféricas, Universidade de São Paulo, São Paulo, Brazil; brenorfs@gmail.com
[2] Instituto de Física, Universidade de São Paulo, São Paulo, Brazil
Received 2019 November 27; revised 2020 January 21; accepted 2020 January 29; published 2020 February 13

Abstract

The long-term solar cycle variability and Grand solar minima remain open questions from a theoretical point of view. Recently, a growing basis of evidence points out to the role of the magnetic Rossby waves in the solar cycle. Here we present a simple deterministic model, based on a low-order spectral representation of the barotropic quasi-geostrophic-magnetohydrodynamic equations for the Solar tachocline. This model supports the idea of the long-term behavior of the solar activity as a result of nonlinear interaction of magnetic Rossby modes. Solutions show that Rossby waves undergo irregular switches between periods of high activity and periods of suppressed activity, resembling the Maunder minimum. Low-energy states in the model are associated with the synchronization of the dynamical phases of the waves. These irregular transitions in the amplitudes of the waves are reminiscent of the observed time series of the solar activity. This suggests that Maunder-like states arise from chaotic transitions between regimes with different degrees of organization in the system.

Unified Astronomy Thesaurus concepts: Solar cycle (1487); Maunder minimum (1015); Sunspot cycle (1650); Magnetohydrodynamics (1964); Chaos (222); Alfven waves (23); Solar magnetic fields (1503)

1. Introduction

In addition to the main approximately 11 yr cycle, observational records have shown that the solar magnetic activity exhibits several modulations on longer timescales of the order of hundreds and thousands of years (Usoskin 2017). A particular phenomenon of great interest in the realm of long-term solar cycle variability is that of Grand solar minima, usually defined as periods in which the solar magnetic activity is strongly suppressed. Among the Grand minimum periods, the most recent and prominent one is the so-called Maunder Minimum (Usoskin et al. 2015) that occurred between the years of 1645 and 1715 when the sunspots were barely visible. Although the Maunder minimum was the only Grand minimum period directly observed, studies based on the reconstruction of the Solar activity of the past Holoscene period through the analysis of cosmogenic isotopes such as ^{14}C and ^{10}Be indicate that there may have been other similar periods in the past. For example, Usoskin et al. (2007) has estimated that one-sixth of Solar activity is spent in such states of low activity.

Apart from the intrinsic scientific interest in the Grand minimum periods, the coincidence between the Maunder minimum and the so-called "little ice age" (a period of extreme cold climate in Europe in the 1600s and 1700s) suggests a possible modulation of Earth's climate by the solar cycle variability (see, for instance, Crowley 2000; Mauquoy et al. 2002; and Owens et al. 2017), which increases the necessity to understand the mechanisms behind the occurrence of a Grand minimum event and consequently to properly model it numerically and ultimately satisfactorily predict its occurrence.

From a theoretical point of view, the mechanisms that have been proposed for the occurrence of Grand minima and the long-term solar cycle modulations are based on either mean-field dynamo models forced by stochastic fluctuations (Ossendrijver 2000) or on-off intermittency behavior in chaotic processes (Platt et al. 1993), although none of these models seem to have firm derivations based on the magnetohydrodynamic (MHD) equations.

On the other hand, the study of the nonlinear MHD Rossby wave interactions in the context of the Solar cycle was introduced in Raphaldini & Raupp (2015), which included evidence for the cyclic modal energy exchange obeying the same timescale of the main ∼11 yr cycle of solar magnetic activity, as well as evidence for the equator-ward propagation in a realistic differential rotation profile in accordance with the observed butterfly diagram. In a more general context of nonlinear wave interaction and wave turbulence, it is usual to consider the so-called "random phase hypothesis" (Zakharov et al. 2012; Nazarenko 2011). This hypothesis has led to a paradigm that the dynamical phases were unimportant to the energy transfers throughout the modal space in a turbulent system. Conversely, there has been a recent growing basis of research pointing out the importance of the wave dynamical phases in the energy transfers among the modal structures in turbulent regimes. Chian et al. (2010) showed in a model of regularized long-wave equation that amplitude-phase synchronization can lead the dynamical system to switching between regular and irregular behaviors, which are measured by a spectral entropy. Their methodology was extended to other turbulent contexts, including MHD effects in Keplerian disks (Miranda et al. 2015). Another important mechanism associated with the dynamics of the wave phases was discovered recently by Bustamante et al. (2014): the so-called "precession resonance mechanism." This mechanism is related to the fact that the oscillation due to the linear phase mismatch in a wave triad can resonate with the nonlinear amplitude oscillation of an adjacent triad, leading to strong transfers of energy throughout the whole modal space. This theory was also extended to include dissipation in the context of Burger equation (Murray & Bustamante 2018), in which bursts of strong energy transfer interchanged with periods of weak interaction were found to be associated with synchronized/unsynchronized regimes in the dynamical phases. Raphaldini et al. (2019) studied the

precession resonance mechanism in the context of MHD Rossby waves in the solar tachocline. They analyzed the reduced dynamics of two interacting wave triads coupled by a single mode and demonstrated that, in the conservative dynamics, the aforementioned precession resonance mechanism maximizes the efficiency of energy transfer between the two connecting triplets, which in turn yields long-term modulations of the main approximately 11 yr cycle associated with the intra-triad energy exchanges. In addition, their numerical results show that the inclusion of forcing and dissipation yields solutions that are reminiscent of the time series of the solar magnetic activity, interchanging between Grand minimum-like periods and periods of strong activity.

Recently, the interest in the magnetic Rossby waves in the context of the solar variability has sparked due to observational evidence for their existence (see, for instance, McIntosh et al. 2017; Löptien et al. 2018). This evidence of magnetic Rossby waves has been based on observed slow oscillations that are believed to be relevant in the tachocline region of the Sun and have been associated with the MHD generalization of the hydrodynamic Rossby waves that govern the dynamics of geophysical fluids (Zaqarashvili et al. 2007). A large number of articles have addressed different aspects of this oscillation type. Dikpati et al. (2017) and Dikpati et al. (2018a) showed that the interaction of Rossby waves with the differential rotation (zonal flow) may produce either bursted or quiet seasons in the Sun. Zaqarashvili (2018) explored the dynamics of these waves in the equatorial region, among other faster types of modes. The association between Rossby waves and solar magnetic fields goes back (Gilman 1969). One important aspect of the Rossby waves in the context of the Sun and other stars is that they can play a role in the dynamo process via alpha effect. The alpha effect is an essential component of the dynamo process that converts toroidal magnetic fields into poloidal ones (Brandenburg & Subramanian 2005). Indeed, Rossby waves are associated with helical motions and, therefore, constitute a good candidate to provide the alpha effect (see also Gilman & Dikpati 2014).

In this Letter we have extended the study of Raphaldini et al. (2019) in order to further investigate the mechanisms associated with the periods of suppressed activity of the mode amplitudes resembling the Grand minimum states of solar magnetic activity that appeared in their forced-dissipative reduced model of nonlinearly interacting MHD Rossby modes. In this context, we have analyzed the sensitivity of the results to the magnitude of the forcing, as well as the time evolution of the fully nonlinear wave phases. We have demonstrated that the synchronization/desynchronization of wave phases leads the dynamics of the corresponding low-dimensional dynamical system to switch between periods of high activity/strong interactions and periods of suppressed activity/weak interactions. Therefore, we suggest that the amplitude-phase synchronization associated with the nonlinear dynamics of MHD Rossby modes at the solar tachocline can be a possible dynamical mechanism responsible for the emergence of Grand minimum-like states of the solar magnetic activity. Consequently, this Letter corroborates with the results of the previous works of Raphaldini et al. (2019) and Raphaldini & Raupp (2015), pointing out the importance of nonlinear MHD Rossby modes at the solar tachocline for the observed magnetic activity of the Sun.

2. Model Equations

The simplest model bearing the existence of magnetic Rossby waves at the solar tachocline corresponds to the MHD generalization of the barotropic non-divergent model (Zaqarashvili et al. 2007), which in turn represents a simplified version of the quasi-geostrophic MHD equations (Zeitlin 2013) with the assumption of high equivalent depth. The MHD generalization of the barotropic non-divergent model can be expressed in terms of the conservation of absolute vorticity and the induction equation in spherical coordinates as follows:

$$\frac{\partial \nabla^2 \psi}{\partial t} + J(\psi, q) = \frac{1}{\mu_0 \rho} J(A, j) \tag{1}$$

$$\frac{\partial A}{\partial t} + J(\psi, A) = 0 \tag{2}$$

In the equations above, ψ is the streamfunction, A is the magnetic potential, $j = \nabla^2 A$ is the magnetic current, and $q = \nabla^2\psi + 2\Omega \sin\theta$ is the absolute vorticity, with Ω referring to the rotation rate of the radiative zone of the Sun; μ_0 is the magnetic permeability of the vacuum, ρ is the density of the plasma at the tachocline region, and θ is the latitude. In our spherical coordinate system the Jacobian nonlinear operator takes the form

$$J(f, g) = \frac{1}{a^2 \cos\theta}\left(\frac{\partial g}{\partial \theta}\frac{\partial f}{\partial \phi} - \frac{\partial f}{\partial \theta}\frac{\partial g}{\partial \phi}\right) \tag{3}$$

where f and g represent two arbitrary functions, ϕ is the longitude, and a is the tachocline solar radius.

As mentioned in the previous section, we consider a highly truncated spectral representation of Equations (1) and (2) in terms of the eigensolutions of their linearized version around a background state at rest (no mean flow) and having a global structure toroidal magnetic field $\boldsymbol{B} = (\mathrm{B}_0 \cos\theta, 0)$, with B_0 being set to yield an Alfvén wave speed of $v_A = B_0/\sqrt{\mu_0 \rho} = 100\ \mathrm{m\ s^{-1}}$. In other words, we have considered the following ansatz:

$$\psi(\phi, \theta, t) = \sum_{j=1}^{5} \Lambda_j(t) \frac{\omega_j}{m_j} Y_{n_j}^{m_j}(\phi, \theta) e^{-i\omega_j t} \tag{4a}$$

$$A(\phi, \theta, t) = \sum_{j=1}^{5} \Lambda_j(t) \frac{B_0}{a} Y_{n_j}^{m_j}(\phi, \theta) e^{-i\omega_j t} \tag{4b}$$

where $\Lambda_j(t)$ refers to the complex valued mode amplitudes, $Y_n^m(\phi, \theta)$ are the eigenfunctions of the Laplace operator (i.e., $\nabla^2 Y_{n_j}^{m_j} = -\frac{n_j(n_j+1)}{a^2} Y_{n_j}^{m_j}$), and the eigenfrequencies ω_j satisfy the following dispersion relation:

$$\omega_j = \frac{1}{2}\left(-\frac{2\Omega m_j}{n_j(n_j+1)} \pm \sqrt{\left(\frac{2\Omega m_j}{n_j(n_j+1)}\right)^2 + \frac{4B_0^2 m_j^2}{\mu_0 \rho a^2}\left(1 - \frac{2}{n_j(n_j+1)}\right)}\right) \tag{5}$$

with the $\pm$ sign indicating the two possible branches, namely the fast hydrodynamic mode ($-$) and the slow magnetic mode ($+$). Indeed, one notices that setting $B_0 = 0$ ($\Omega = 0$) recovers the dispersion relation of Rossby–Haurwitz (Alfvén) waves,

Table 1
Wavenumbers and Corresponding Eigenfrequencies of the Selected Waves in the Five-wave Model, Separated in Two Triads (a and b)

Wavenumber (1)	Frequency(Hz) (2)	Triad (3)	Triad Coefficient (4)	Dissipation Parameter (5)
(0, 2)	0	a	−0.200293 i	1.02^{-17}
(1, 10)	$1.78236 * 10^{-7}$	a	−1.75195 i	1.14^{-17}
(1, 9)	$1.72695 * 10^{-7}$	a	−2.15463 i	9.54^{-18}
(1, 9)	$1.72695 * 10^{-7}$	b	0.620163 i	9.54^{-18}
(1, 12)	$1.85859 * 10^{-7}$	b	0.27978 i	1.56^{-17}
(2, 10)	$3.56473 * 10^{-7}$	b	0.904184 i	1.14^{-17}

Note. The corresponding frequency mismatches give $1/\delta_a = 5.72248$ yr and $1/\delta_b = 15.2326$ yr. All the parameter values are in MKS units.

which is compatible with the linear theory results of Zaqarashvili et al. (2007) obtained directly from the shallow-water MHD equations. Once a vorticity source[3] and dissipation are included in (1) and (2), plugging (4a) and (4b) into these equations yields a low-dimensional dynamical system governing the time evolution of the mode amplitudes, viz.

$$\frac{d\Lambda_1}{dt} = C_{1,2,3}\Lambda_2^*\Lambda_3 e^{i\delta_a t} - d_1\Lambda_1 \tag{6}$$

$$\frac{d\Lambda_2}{dt} = C_{2,3,1}\Lambda_1^*\Lambda_3 e^{i\delta_a t} - d_2\Lambda_2 \tag{7}$$

$$\frac{d\Lambda_3}{dt} = f_3 + C_{3,1,2}\Lambda_1\Lambda_2 e^{-i\delta_a t} + C_{3,4,5}\Lambda_4\Lambda_5 e^{-i\delta_b t} - d_3\Lambda_3 \tag{8}$$

$$\frac{d\Lambda_4}{dt} = C_{4,3,5}\Lambda_5^*\Lambda_3 e^{i\delta_b t} - d_4\Lambda_4 \tag{9}$$

$$\frac{d\Lambda_5}{dt} = C_{5,3,4}\Lambda_4^*\Lambda_3 e^{i\delta_b t} - d_5\Lambda_5 \tag{10}$$

In the equations above, the superscript "$*$" indicates the complex conjugate, $\delta_a = \omega_1 - \omega_2 - \omega_3$ and $\delta_b = \omega_5 - \omega_3 - \omega_4$ refer to the linear frequency mismatches of Triads a (Modes 1, 2, and 3) and b (Modes 3, 4, and 5), respectively; $C_{j,l,k}$ are the nonlinear coupling constants, f_j refers to the projection of the vorticity forcing onto each wave mode,[4] and d_j, $j = 1, 2, 3, 4$, and 5, are the damping coefficients. Details on the derivation of the equations above, including the expressions of coefficients $C_{j,k,l}$, f_j and d_j, as well as the selection rules required for the nonlinear coupling coefficients to be nonzero, can be found in Raphaldini et al. (2019).

3. Results

A representative example of two wave triplets coupled by a common wave mode, whose spectral amplitudes satisfy system (6)–(10), is illustrated in Table 1. The linear frequency mismatch of Triad a is associated with an oscillation period of approximately a half of the main ∼11 yr period of the solar cycle. Raphaldini et al. (2019) showed a numerical integration of system (6)–(10) in the precession resonance regime, in which the amplitude oscillation of Triad b, which is nearly resonant, resonates with the linear frequency mismatch of Triad a. The numerical results presented in Raphaldini et al. (2019) for an arbitrary value of the forcing parameter f_3 display a time series of Mode 3 amplitude that is reminiscent with the time series of the solar magnetic activity, showing periods of suppressed activity that resemble the Grand minima. Here we further analyze the numerical results of system (6)–(10) to better understand the mechanism behind the occurrence of such periods of low-amplitude fluctuations and, consequently, to yield a theoretical description of the Grand minima of solar magnetic activity based on the nonlinear dynamics of magnetic Rossby waves at the solar tachocline.

Figure 1 shows the time evolution of the amplitude $|A_j(t)| = \sqrt{A_j A_j^*}$, $j = 1, 2, 3$, of the spectral coefficients of the modes of Triad a for two regimes, one with forcing and dissipation, namely $f_3 = 2.08 \times 10^{-17}$, and the second without forcing and dissipation. As in Raphaldini et al. (2019), the regime of the spectral amplitudes displayed in Figure 1 (precession resonance regime) maximizes the energy transfer between the two triads. Thus, regardless of the forcing parameter value, the mode amplitudes $|A_j|$, $j = 1, 2, 3$, undergo fluctuations with a main period of the order of 10 yr. This main ∼10 yr oscillation is associated with the energy exchanges among the modes of the same triplet (Modes 1, 2, and 3, for instance) and is compatible with the main frequency of the solar cycle. This main ∼10 yr oscillation of the spectral amplitudes is modulated by longer timescale fluctuations that result from energy transfers between the two different triads. This main amplitude fluctuation with an approximately 10 yr period, alternating smaller and larger peaks on longer timescales ranging from several hundred to a few thousand years, is in agreement with observational records of the solar activity. For instance, Usoskin (2017) pointed out the following well-defined long-term variability modes of the solar magnetic activity: the Gleinsberg cycle with timescale of approximately 100 yr, the Suess de Vries cycle of approximately 200 yr, the Millennial Eddy cycle at the timescale of 1000 yr, and the Hallstatt cycle with an approximately 2400 yr period.

Conversely, depending on the value of the forcing parameter, f_3, system (6)–(10) can undergo recurrent periods with very low energy. In fact, in the numerical integration with forcing and dissipation presented in Figure 1 (left panel) one observes recurrent periods of very low energy of the first triad (i.e., $E \sim |A_1|^2 + |A_2|^2 + |A_3|^2$). Such periods resemble the dynamics of the so-called Grand minima in the observational record of the magnetic activity of the Sun. In contrast, in the numerical integration in the conservative case (right panel of Figure 1), these low-energy states are no longer observed. For other values of the forcing parameter (not shown here), the duration and the recurrence of such periods of low energy differ considerably, from very short and more rare low-energy periods to more persistent and recurrent periods.

In addition to analyzing the behavior of the amplitudes of the spectral coefficients, it is also important to investigate the dynamics of their phases. As discussed in Section 1, recent studies have shown that the mode phases play an important role in the nonlinear interaction of the waves (Bustamante et al. 2014). In particular, the dynamics of the wave phases are directly associated with an intermittent-type behavior of dynamical systems describing the nonlinear dynamics of

[3] The vorticity source included in (1) refers to the linear divergence term of the vorticity balance (see Raphaldini & Raupp 2015 for details), and can be thought of as representing the effects of either baroclinic instability (Gilman & Dikpati 2014) or thermal anomalies at the top of the radiative zone.

[4] For simplicity, here we have assumed that the forcing projects only onto Mode 3.

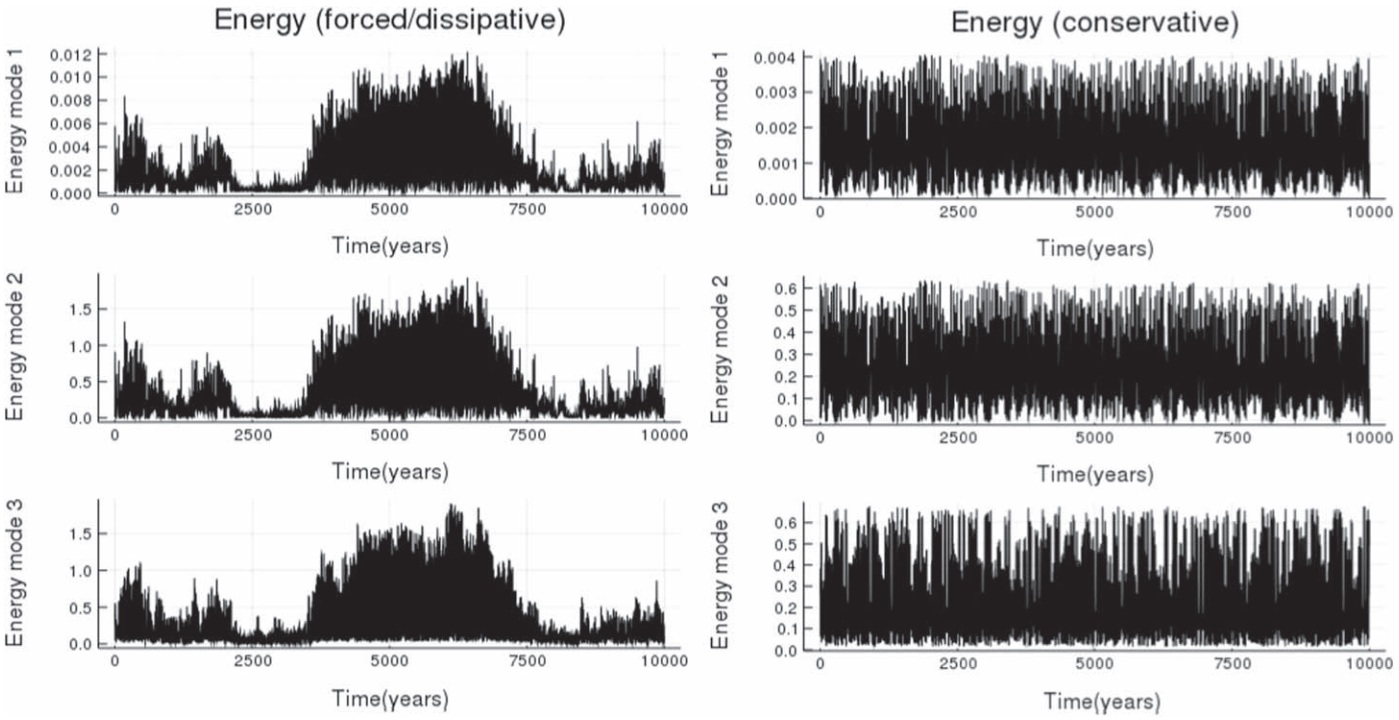

Figure 1. Time evolution of the energies in each mode $E_j = A_j A_j^*$, $j = 1, 2, 3$, of Triad a, for the forced/dissipative case (left panel) and for the conservative case (right panel), over a 10,000 year period. One observes long-term modulations with timescales of several hundred/thousand years on the amplitude peaks of the main ~10 yr cycle in the case with forcing and dissipation. One notices in this case the occurrence of periods of very low energy of the three wave modes, whereas for conservative case (right panel) one does not observe such periods.

interacting wave modes (Chian et al. 2010; Murray & Bustamante 2018). In addition, the time series of observed solar activity exhibits a remarkable intermittent behavior (Usoskin 2017). Thus, Figure 2 shows the time evolution of the phase difference among the modes, $\delta\phi(t) = \phi_3(t) - \phi_2(t) - \phi_1(t) + \phi_4(t) - \phi_5(t)$. This phase difference is illustrated in Figure 2 without the multiples of 2π to remove its singular growth at these points. The evolution of the phase difference observed in Figure 2 switches between a fast-growing phase and phase-locked or slowly growing phase periods. By comparing the time evolution of the phase difference, $\delta\phi$, with the time evolution of the amplitudes of the modes of the first triad,[5] one notices that the phase-locked/slowly growing periods coincide with periods of low energy of the modes, as can be clearly noticed in Figure 2 (top panel). This coincidence suggests that, if we define an instantaneous frequency mismatch by $\delta\omega(t) = d(\delta\phi(t))/dt$, one would expect that this instantaneous frequency mismatch be proportional to the amplitude of the second mode, as can be confirmed in Figure 2 (bottom panel). Since the signal is too noisy, we present a smoothed version of the time series of $\delta\omega(t)$ together with the amplitude of Mode 2 in Figure 2 (bottom panel), where one can observe: (i) the coincidence of synchronized periods (low dynamical mismatch $\delta\omega(t)$) with periods of low-energy states, and (ii) the coincidence of periods when $\delta\omega(t)$ is large with periods of high amplitude of the modes of the first triad. By analyzing the phase-space projection onto the plane $\mathrm{Re}\,A_2 \times \mathrm{Im}\,A_2$ (Figure 3), one can see that the synchronized state (bottom panel) is associated with an inhibited propagation regime of Mode 2, whereas a normal unsynchronized period is associated with a regular propagation regime of this mode. Therefore, the synchronization mechanism presented here acts to decrease the effective (nonlinear) phase speed of Mode 2 such that the difference between its nonlinear frequency and the nonlinear frequency of the other modes becomes small in the synchronized regime.

By analyzing the statistical distribution of the solar activity, Usoskin et al. (2014) suggested the existence of two distinct activity modes evidenced by the bimodal statistical distribution of the reconstructed solar activity time series. Our model presents a similar bimodal behavior, as can be evidenced with the distribution histogram of $\delta\omega(t)$ illustrated in Figure 4 (left panel). As in Chian et al. (2010) there are two states in the system, both chaotic, but one of them more organized (and predictable) than the other. Following the approach of Chian et al. (2010) we evaluated the Shannon entropy of the statistical distribution of frequency mismatches in 200 yr windows:

$$\mathcal{S}(P_T) = -\sum_{t=T-100}^{T+100} P_T(\delta\omega(t)) ln[P_T(\delta\omega(t))], \qquad (11)$$

where $\mathcal{S}$ denotes the Shannon entropy, P_T is the probability distribution of the frequency mismatch at time T. In Figure 4 (right panel), we showed that the Shannon entropy closely follows the frequency mismatch curves with a negative correlation (note the inverted axis in the entropy scale). Since the Shannon entropy is a measure of organization of the system we can conclude that transitions from "normal" to Maunder-like states in the toy model correspond to a transition from a more-organized to a less-organized regime.

[5] For the purpose of clarity, only the amplitude of Mode 2 is displayed.

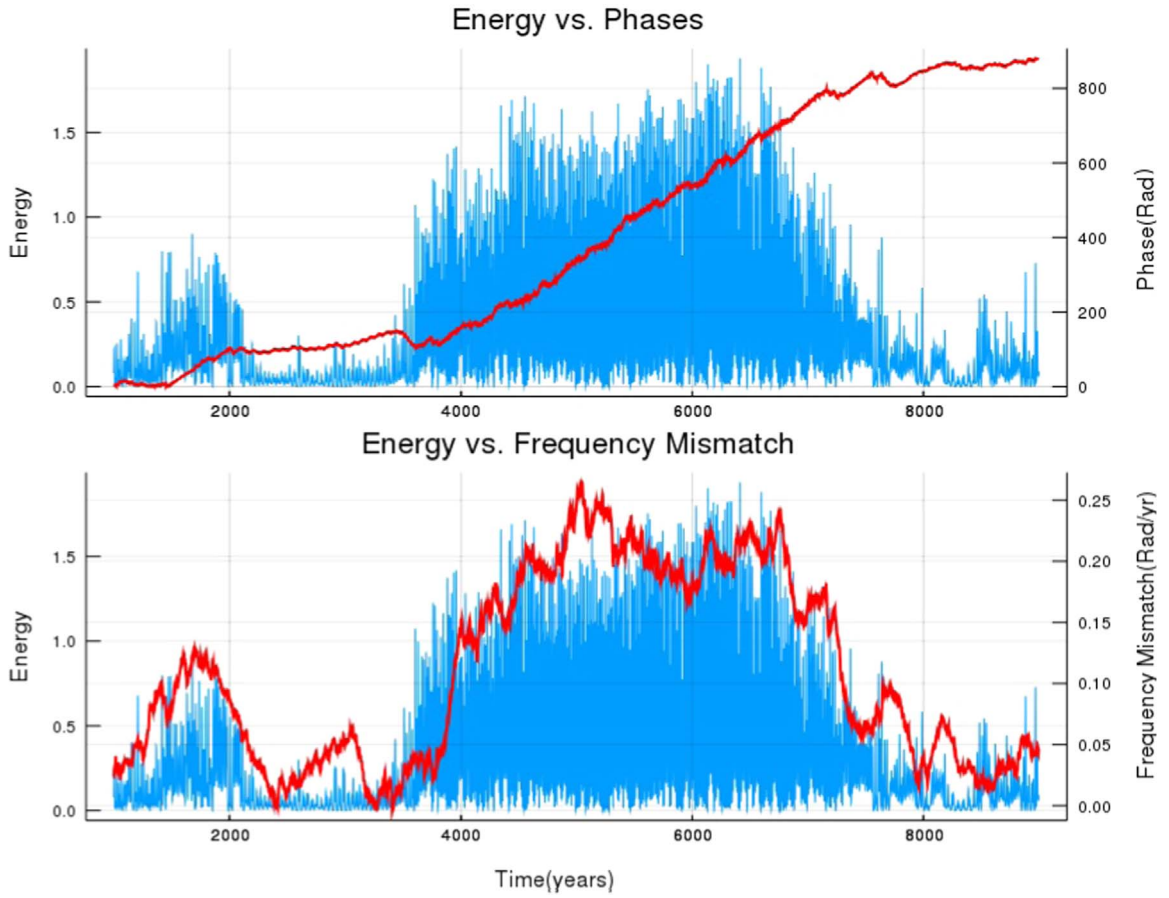

Figure 2. Top panel: the time evolution of the amplitude $|A_2(t)|$ of Mode 2 (blue line) and the modal phase difference $\delta\phi(t) = \phi_3(t) - \phi_2(t) - \phi_1(t) + \phi_4(t) - \phi_5(t)$ (brown line) referred to the same numerical integration illustrated in the left panel of Figure 1 (i.e., for the value of the forcing parameter $f_3 = 2.08 \times 10^{-17}$), but over a shorter period around a prevalent low-energy state. Bottom panel: the time evolution of $|A_2(t)|$ is plotted together with the instantaneous frequency mismatch $\delta\omega$ (see the text). The frequency mismatch is divided by 10 in order to fit the same scale as the amplitude. It is observed that the modal phases become locked for an extended period of time when the energy is very low, unlike the periods of very strong activity in which the phase difference grows faster.

4. Final Remarks

We extended the study of Raphaldini et al. (2019) in order to investigate the mechanisms associated with the periods of suppressed activity of wave amplitudes. Such periods resemble the Grand minimum states that are noticeable in observational records of the Solar magnetic activity. We demonstrated that the suppression of the mode energies is associated with a regime of synchronized wave phases. In these regimes, the mismatch of wave phases becomes locked or drifts very slowly. By contrast, the phase mismatch grows much faster during periods of large mode energies. Similar synchronization mechanisms are also reported in other astrophysical and plasma contexts (see Chian et al. 2010; Miranda et al. 2015; and Rempel et al. 2009). Therefore, we suggest that the amplitude-phase synchronization of Rossby modes at the solar tachocline is a possible dynamical mechanism for the emergence of Grand minimum states in the solar magnetic activity. Consequently, this Letter corroborates with the results of the previous works of Raphaldini et al. (2019) and Raphaldini & Raupp (2015), pointing out the importance of nonlinear MHD Rossby modes at the solar tachocline for the magnetic activity of the Sun.

The model presented here contrasts with stochastic models of the long-term behavior of the Solar activity. Most of these models describe the long-term modulations of the Solar activity driven by stochastic variations of model parameters, most notably the α effect in mean-field dynamos. Arising as a consequence of a random process in these models, states such as grand Solar minima are unpredictable. Since our model is deterministic, although chaotic, it possesses some degree of predictability. This is compatible with the analysis of the available records according to Moss et al. (2008); see also Usoskin (2017).

It remains an open question whether Grand minima are associated with a different state of the Solar dynamo, as pointed out by Usoskin et al. (2014). Our model suggests the existence of at least two separate regimes of the system. In one of these regimes, as system evolves it becomes trapped for long periods in regions of the phase space where the amplitudes of the waves are very low. In these regions, the wave phases become locked, with their mismatch becoming approximately constant for a long time. This poses a strong constraint to the theory proposed here. According to our results, in a Grand minimum state one would expect structures propagating with different velocities compared with a period of normal variability, probably exhibiting slowly propagating or essentially steady structures such as more predominant preferential longitudes.

In the present study we have presented the ideas in a simplified setting, with only five waves and an idealized static

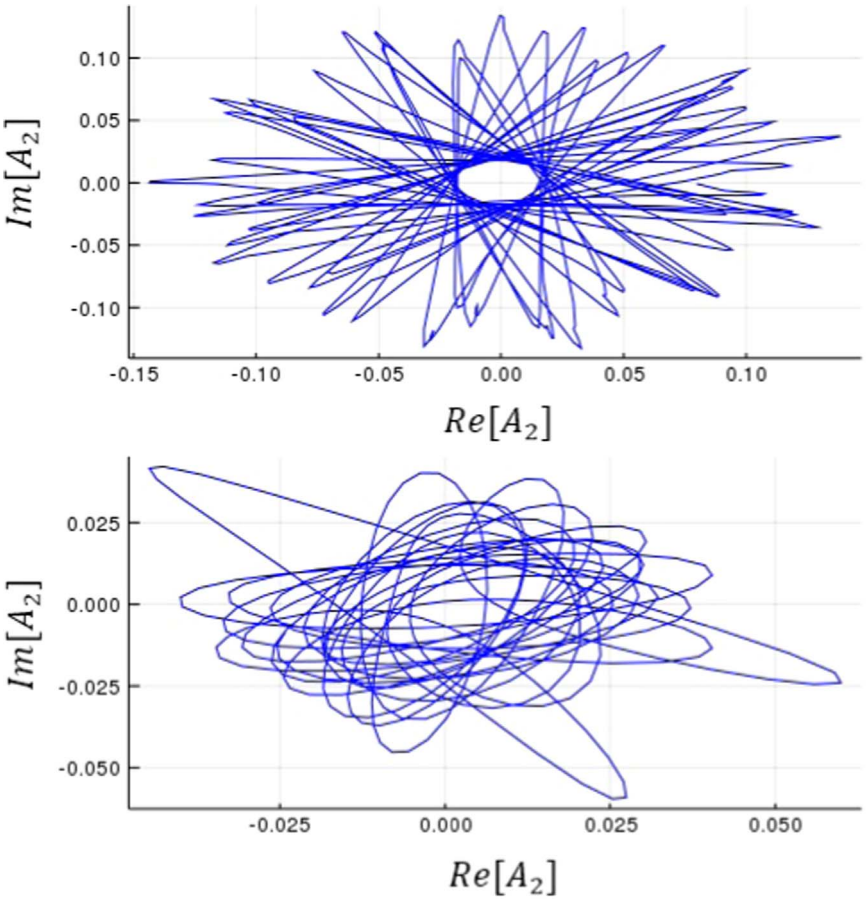

Figure 3. Trajectories in a projection of the phase space (real vs. imaginary parts of Mode 2 amplitude). The top panel refers to a "normal" period, and the bottom panel to a synchronized period. One notices that this particular mode switches from a regular to an irregular propagation regime.

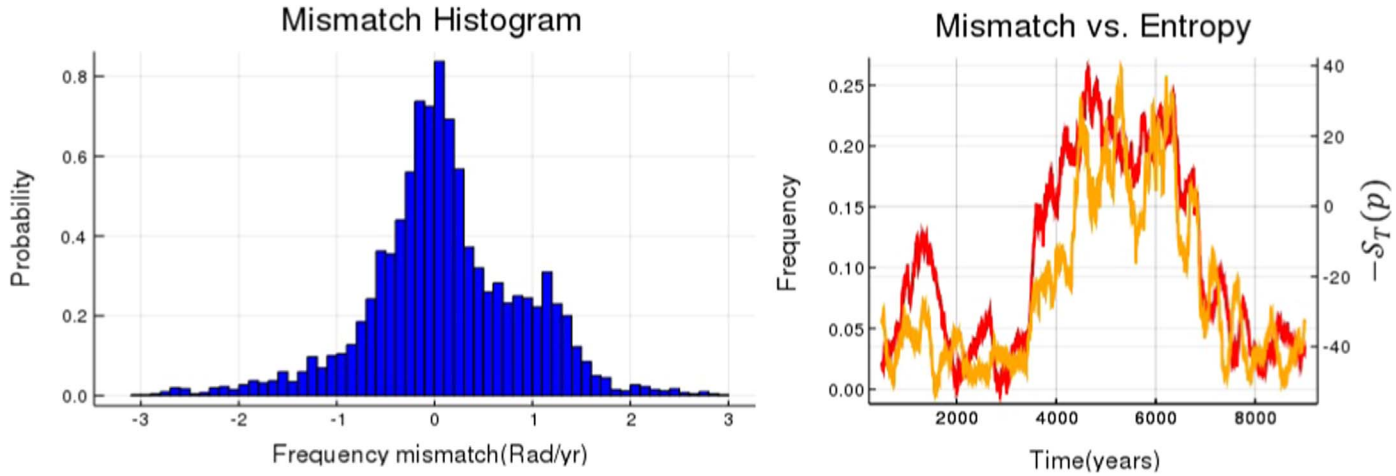

Figure 4. Histogram of the instantaneous frequency mismatch $\delta\omega$ referred to the same numerical solution of Figure 1 (left panel). It is evident that the system has a bimodal character. The evolution of the Shannon Entropy of the system compared with the frequency mismatch curve (right panel).

toroidal magnetic field. A more realistic model should take into account dynamo effects, in particular the asymmetric structure of the toroidal magnetic field that reverses direction according to the dynamo cycle. This type of oscillatory background state can give rise to an MHD analog of the modulational instability explored by Connaughton et al. (2010). The study of unstable Rossby modes under an oscillatory background toroidal magnetic field may provide a selection criterion of the most relevant Rossby modes (i.e., unstable wavenumbers) for the mechanism proposed here, and could also be relevant to shorter-term solar oscillations (Dikpati et al. 2018b, 2018c). Another important extension of this study is the investigation of the role of Rossby waves in the dynamo process. Rossby waves are known to be associated to the alpha effect; such a study could be performed in a model taking into account the role of poloidal fields and stratification (see Avalos-Zuniga et al. 2009 for a Rossby wave-driven dynamo in the context of the geodynamo). The extension of this idea to more complete

models and its comparison with the observational record is necessary to test the hypothesis raised in this article.

The research reported here has received financial support from FAPESP (Fundação de Amparo à Pesquisa do Estado de São Paulo; grants 2015/50686-1, 2017/23417-5, and 2018/03211-6), and CAPES IAG/USP PROEX (grant 0531/2017).

References

Avalos-Zuniga, R., Plunian, F., & Rädler, K. 2009, GApFD, 103, 375
Brandenburg, A., & Subramanian, K. 2005, PhR, 417, 1
Bustamante, M. D., Quinn, B., & Lucas, D. 2014, PhRvL, 113, 084502
Chian, A. C. L., Miranda, R. A., Rempel, E. L., Saiki, Y., & Yamada, M. 2010, PhRvL, 104, 254102
Connaughton, C. P., Nadiga, B. T., Nazarenko, S. V., & Quinn, B. E. 2010, JFM, 654, 207
Crowley, T. J. 2000, Sci, 289, 270
Dikpati, M., Belucz, B., Gilman, P. A., & McIntosh, S. W. 2018a, ApJ, 862, 159
Dikpati, M., Belucz, B., Gilman, P. A., & McIntosh, S. W. 2018b, ApJ, 862, 159
Dikpati, M., Cally, P. S., McIntosh, S. W., & Heifetz, E. 2017, NatSR, 7, 14750
Dikpati, M., McIntosh, S. W., Bothun, G., et al. 2018c, ApJ, 853, 144
Gilman, P. A. 1969, SoPh, 9, 3
Gilman, P. A., & Dikpati, M. 2014, ApJ, 787, 60
Löptien, B., Gizon, L., Birch, A. C., et al. 2018, NatAs, 2, 568
Mauquoy, D., van Geel, B., Blaauw, M., & van der Plicht, J. 2002, Holoc, 12, 1
McIntosh, S. W., Cramer, W. J., Marcano, M. P., & Leamon, R. J. 2017, NatAs, 1, 0086
Miranda, R. A., Rempel, E. L., & Chian, A. L. 2015, MNRAS, 448, 804
Moss, D., Sokoloff, D., Usoskin, I., & Tutubalin, V. 2008, SoPh, 250, 221
Murray, B. P., & Bustamante, M. D. 2018, JFM, 850, 624
Nazarenko, S. 2011, Wave Turbulence, Vol. 825 (Berlin: Springer)
Ossendrijver, M. A. J. H. 2000, A&A, 359, 364
Owens, M. J., Lockwood, M., Hawkins, E., et al. 2017, JSWSC, 7, A33
Platt, N., Spiegel, E. A., & Tresser, C. 1993, GApFD, 73, 147
Raphaldini, B., & Raupp, C. F. M. 2015, ApJ, 799, 78
Raphaldini, B., Teruya, A., Raupp, C. F. M., & Bustamante, M. 2019, ApJ, 887, 1
Rempel, E. L., Proctor, M. R., & Chian, A. C.-L. 2009, MNRAS, 400, 509
Usoskin, I. G. 2017, LRSP, 14, 3
Usoskin, I. G., Arlt, R., Asvestari, E., et al. 2015, A&A, 581, A95
Usoskin, I. G., Hulot, G., Gallet, Y., et al. 2014, A&A, 562, L10
Usoskin, I. G., Solanki, S. K., & Kovaltsov, G. A. 2007, A&A, 471, 301
Zakharov, V. E., L'vov, V. S., & Falkovich, G. 2012, Kolmogorov Spectra of Turbulence I: Wave Turbulence (Berlin: Springer)
Zaqarashvili, T. 2018, ApJ, 856, 32
Zaqarashvili, T. V., Oliver, R., Ballester, J. L., & Shergelashvili, B. M. 2007, A&A, 470, 815
Zeitlin, V. 2013, NPGeo, 20, 893